

Effects of Wall Embedded Length Ratio and Wall Thickness Ratio on Undrained Stability of Cantilever Piled Walls

Boonchai UKRITCHON*, Kant TEERAVONG and Suraparb KEAWSAWASVONG

Department of Civil Engineering, Chulalongkorn University, Bangkok 10330, Thailand

(* Corresponding author's e-mail: boonchai.uk@gmail.com)

Received: 15 June 2015, Revised: 29 October 2015, Accepted: 15 November 2015

Abstract

This paper presents a parametric study of the undrained stability of cantilever piled walls embedded in homogeneous clay. The cantilever piled walls are modeled by the 2 dimensional plane strain condition, and their analyses are carried out by the commercial finite element software, PLAXIS2D. The piled wall is considered to have finite thickness, and thus is also modeled as a volume element with the Mohr-Coulomb material. The strength reduction method is used to simulate the limit state or failure condition of a cantilever piled wall in finite element analysis. The dimensional input parameters of this problem include excavated depth (H), embedded length (L), thickness of piled wall (D), soil unit weight (γ), and undrained shear strength (s_u). The results of this study are summarized in the form of design charts of dimensionless parameters, including stability number ($\gamma H/s_u$), wall embedded length ratio (L/H), wall thickness ratio (D/H), ratio of maximum shear force ($V_{max}/s_u D$), and ratio of maximum bending moment ($M_{max}/s_u D^2$). For the stability number, it was found that L/H has more significant effects on this term than D/H. For both ratios of maximum shear force and maximum bending moment, an increase in L/H and D/H give rise to nonlinear increases and decreases in those ratios, respectively. Some differences in stability number between plate and solid element modelling can be observed in different ratios of wall thickness.

Keywords: Numerical analysis, finite element, piled wall, stability, failure, retaining structure

Introduction

Retaining walls are structures which resist lateral earth pressure when there are significant changes of soil movement and the soil cannot maintain its stability. At present, there has been an increase in the use of piled retaining walls for excavations in practice, since underground constructions are so deep that retaining walls are required to maintain stability. Designs and constructions of retaining walls are very important, in order to ensure an adequate safety factor, and retaining walls are economical. In general, analyses of retaining walls in cohesive clays are based on the classical limit equilibrium method from the equilibrium of lateral earth pressure on both sides of retaining walls. In addition, commercial software is employed to determine shear force and bending moment in the walls, lateral wall deflection, or ground movement. **Figure 1** shows an example of a piled retaining wall, used as a temporary structure to resist soil movement, in the basement construction of a project in Bangkok, Thailand (Thasnanipan *et al.* [1]).

In general, stability analyses of retaining walls in geotechnical engineering are normally represented in terms of stability number ($N = \gamma H/s_u$), where γ = unit weight of soil, H = excavated height, and s_u = undrained shear strength of clay. Some important solutions of stability numbers for excavations in clay layers include Terzaghi [2], Bjerrum & Eide [3], Eide *et al.* [4], O'Rourke [5], Ukritchon *et al.* [6], and Khatri and Kumar [7]. For an unsupported vertical cut in clay, Martin [8] used the numerical methods of lower and upper bound limit analyses to determine a very accurate bound solution of this problem, being:

$N = 3.7764904 - 3.7764911$. Thus, this number can be referred to as the exact solution of an unsupported vertical cut in clay. **Figure 2** shows the slip line solution of an unsupported vertical cut by Martin [8]. It should be noted that the stability number of an unsupported vertical cut in clay is a fundamental solution which serves as a basis for studying a more complex problem concerning retaining walls in cohesive soil, such as propped walls or braced excavation. Those complex problems shall have a stability number more than that of an unsupported vertical cut, because of the effects of wall embedded length and bracing.

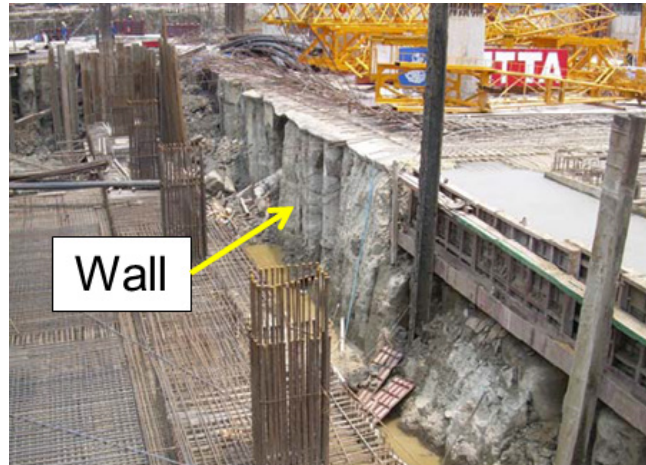


Figure 1 Example of piled retaining wall in practice as temporary structure of basement construction, Thasnanipan *et al.* [1].

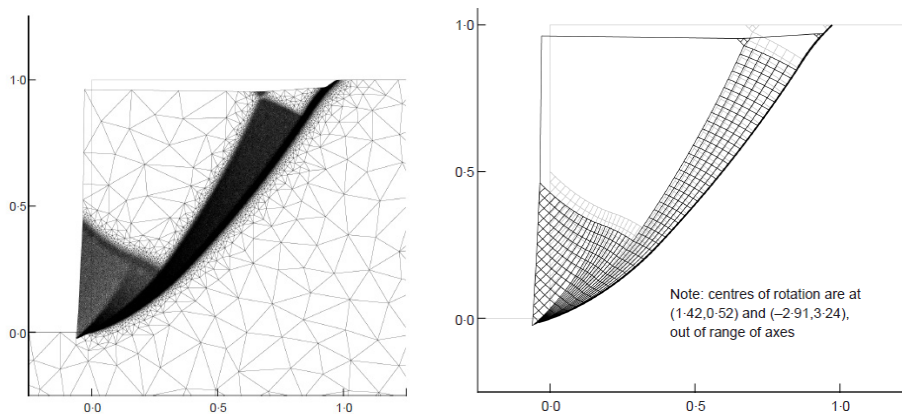


Figure 2 Slip line solution of unsupported vertical cut from finite element limit analyses, Martin [8].

Even though there have been numerous studies of retaining walls by means of limit equilibrium, limit analysis, and finite element method, studies of wall thickness effects have been limited. In particular, studies of the undrained stability of piled walls are very few, but there have been significant increases in applications of this retaining wall in practice, as shown in **Figure 1**. Therefore, the topic and research work of this study is still important and required for the future.

works by Fliz and Navin [10] and Yang [11]. The piled wall is assumed to be made of a mixture of soil and cement, which has its unit weight approximately equal to the surrounding clay layer, γ , and the Poisson's ratio, ν is about 0.25. Its unconfined compressive strength of soil-cement wall, f'_c , is about 600 kPa (5 % cement content). Thus, the piled wall has a total cohesion of $s_u = f'_c/2$ with the $\phi = 0$ concept and the associated flow rule. The Young's modulus of the piled wall is approximated by an empirical equation as: $E_{\text{wall}} = 1520000(f'_c/100)^{0.5}$, all units in kPa.

The interaction between the clay and the pile wall is modeled by interface elements, including both sides around the wall and at the bottom plane. Interface roughness between the clay and piled wall is set to 0.667, which is a typical value for soil-structure interface. The boundary displacement conditions on both the left and right sides are zero movement in a horizontal direction ($u_x = 0$) while the vertical movements are free. At the bottom plane of the model, both horizontal and vertical displacements are set to zero ($u_x = u_y = 0$). The top ground surface of the retained and excavated sides is free to move in both directions ($u_x \neq 0, u_y \neq 0$). The dimensions of the domain are chosen to be large enough that the failure zone does not intersect the boundaries, and thus they do not have any effect on the computed results.

Figure 3 also shows the numerical model geometry consisting dimensional parameters, namely excavated depth (H), embedded length (L), and thickness of the piled wall (D). Forces in the piled wall are evaluated after failure analysis, including maximum shear force (V_{max}) and maximum bending moment (M_{max}).

Both clay and piled wall elements are discretized by 15 noded triangular elements, corresponding to the cubic strain element type. The soil-structure interface has 10 nodes for each element. **Figure 4** shows examples of finite element meshes used in the analyses. Very fine mesh element distribution is used for all cases, in order to obtain accurate solutions of the limit state analysis.

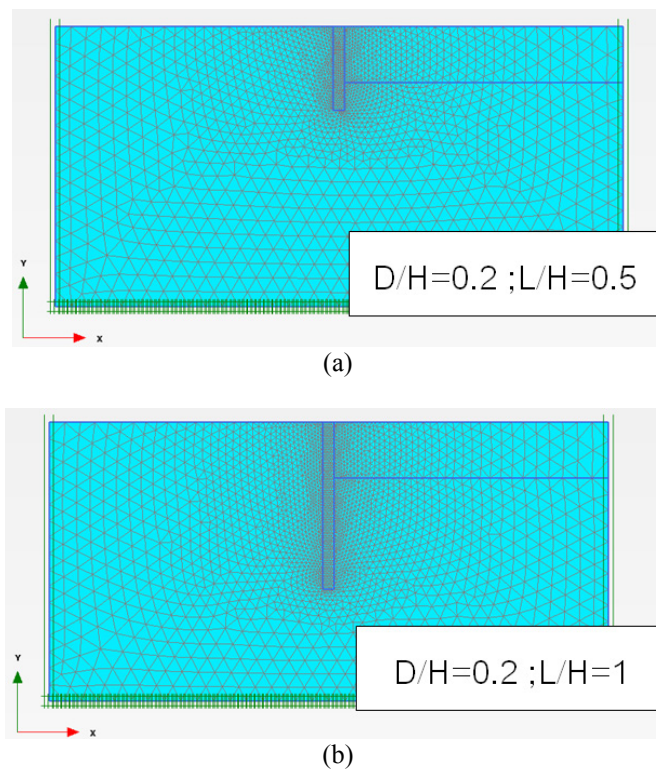


Figure 4 Examples of finite element mesh of piled wall in stability analysis, (a) $D/H = 0.2; L/H = 0.5$, (b) $D/H = 0.2; L/H = 1$.

Failure analyses of the piled wall are performed by means of the strength reduction method or the Phi-c reduction method, giving rise to the value of safety factor (FS). In this method, the full undrained shear strength of the clay is successively and automatically reduced by the safety factor. The limit state or failure state occurs when FS converges to a constant value and the final corresponding safety factor is obtained after the analysis. As a result, the mobilized undrained shear strength can be calculated from the concept of the strength reduction method together with the factor of safety as;

$$FS = s_{ui}/s_u \quad (1)$$

$$s_u = s_{ui}/FS \quad (2)$$

where, s_{ui} = inputted full undrained shear strength in the finite element software

s_u = mobilized undrained shear strength

FS = factor of safety

Undrained stability analyses of the cantilever piled wall are performed by varying dimensional parameters as: H, L, D, γ , s_u , and the corresponding computed results are: FS, V_{max} and M_{max} . However, the independent dimensionless parameters can be formed from those variables based on the technique of dimensionless analysis [12]. Thus, the cantilever piled wall has 2 dimensionless input parameters:

1) Wall embedded length ratio (L/H)

2) Wall thickness ratio (D/H)

The practical ranges of input dimensionless parameters are studied as: L/H = 0.5 - 2 and D/H 0.12 - 0.33.

The output dimensionless parameters include 3 terms:

1) Stability number ($\gamma H/s_u$)

2) Ratio of maximum shear force ($V_{max}/s_u D$)

3) Ratio of maximum bending moment ($M_{max}/s_u D^2$)

Thus, the output dimensionless parameters can be written in terms of input dimensionless parameters as;

$$\gamma H/s_u = f(L/H, D/H) \quad (3)$$

$$V_{max}/s_u D = g(L/H, D/H) \quad (4)$$

$$M_{max}/s_u D^2 = h(L/H, D/H) \quad (5)$$

Figure 5 shows examples of stage analysis in the finite element simulation. Basically, there are 4 stages in the analysis. The first stage corresponds to the stage of setting up an initial state of stress in the soil mass by the gravity force calculation of the K_0 -condition method (**Figure 5a**). Next, the piled wall and its surrounding interfaces are activated in the second stage (**Figure 5b**). The third stage is to deactivate the excavated soil part for simulating the excavation process (**Figure 5c**). The last stage is to analyze the limit or failure state by means of the strength reduction method, giving rise to the corresponding factor of safety for all input dimensional variables. Then, input and output dimensionless parameters are determined for each case of parametric study.

It should be noted that the limit state of the problem is governed by only the failure in the clay layer. For all cases, there is no failure happening in the piled wall, since the undrained shear strength of the clay layer is relatively low compared to the total cohesion of the piled wall calculated from its confined compressive strength as described earlier. The values of Young's modulus of the clay and the piled wall do not affect on stability number, ratios of maximum shear force and maximum bending moment at the limit state.

Figure 6 shows an example result of iterative calculations by the strength reduction method for the failure state simulation. In order to ensure that the limit state is successfully reached in the analysis, the curve of the factor of safety must reach the state of convergence at the last step of calculation. Thus, this curve is verified for all cases of parametric studies, such that the true collapse solutions are solved and are not affected by some other effects of numerical problems associated with finite element calculations.

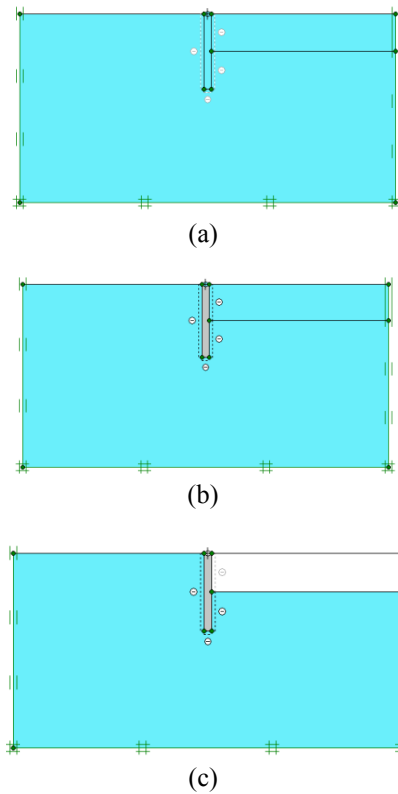


Figure 5 Examples of stage analyses of cantilever piled wall stability (a) Initial stage: K0-procedure, (b) Activate wall and interface, (c) Excavate soil.

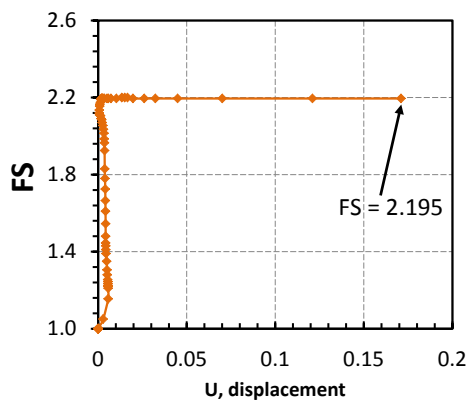


Figure 6 Example result of iterative calculations by the strength reduction method.

Results and discussion

All solutions of parametric studies are summarized in the form of design charts of dimensionless parameters as described in the previous section, namely stability number ($\gamma H/s_u$), ratio of maximum shear force ($V_{max}/s_u D$), and ratios of maximum bending moment ($M_{max}/s_u D^2$) as a function of embedded length ratio (L/H) and wall thickness ratio (D/H). The studied ranges of input dimensionless parameters are: $D/H = 0.5, 1.0, 1.5, 2.0$, and $L/H = 0.12, 0.15, 0.16, 0.20, 0.25, 0.27, 0.33$.

Stability number

Figure 7 shows the relationship between $\gamma H/s_u$ and L/H for the series contours of D/H . The results are replotted again between $\gamma H/s_u$ and D/H for the series contours of L/H . Two different charts enable more understanding of these 2 parameters D/H and L/H on how they affect the stability number. Generally, the stability number of the piled wall cases is in the range of $\gamma H/s_u = 4.55 - 4.90$. These ranges are larger than that of an unsupported vertical cut case reported by Martin [8], $\gamma H/s_u = 3.776$, because of the presence and influence of the piled wall. In addition, the effect of wall embedment, L/H , is quite significant on the stability number. The deeper wall embedment ratio is related to the higher stability number. However, the effect of wall thickness is not significant, when compared to the effect of wall embedment. Wall thickness significantly increases stability number in the case of shallow embedded length. On the other hand, there is only a very small increase of stability number in the case of deep embedment length due to wall thickness.

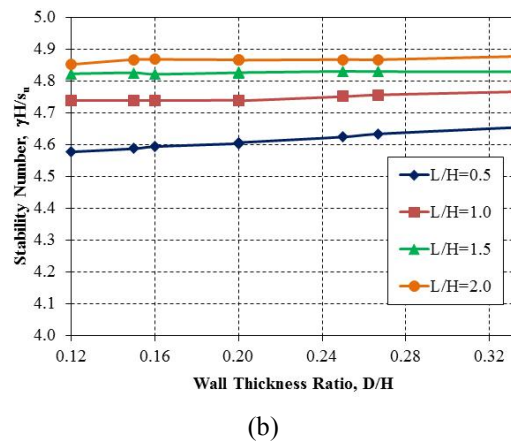
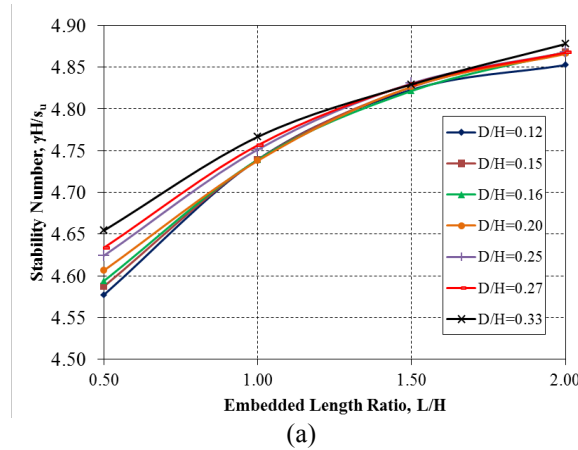
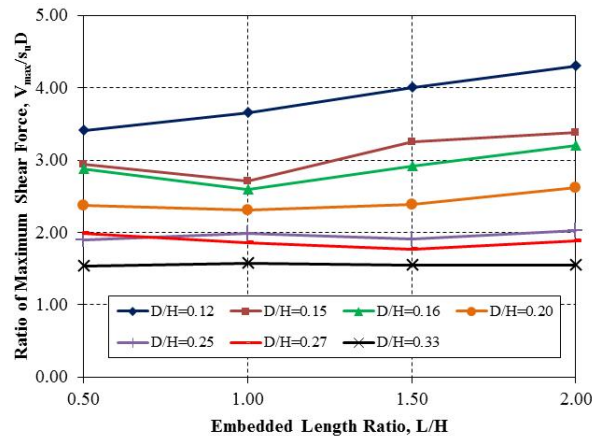


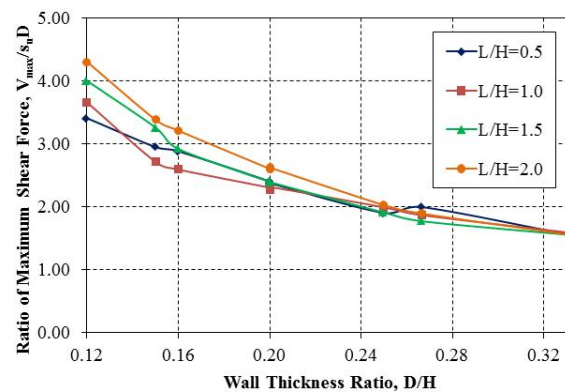
Figure 7 Stability number of cantilever piled walls, a) $\gamma H/s_u$ vs. L/H b) $\gamma H/s_u$ vs. D/H .

Ratio of maximum shear force

Figure 8 shows the ratio of maximum shear force (V_{max}/s_uD) as a function of embedded length ratio (L/H) and wall thickness ratio (D/H). These 2 design charts show the effects of dimensionless parameters, L/H and D/H , on the forces generated in piled walls at the limit state. There is only a small increase in maximum shear force ratio when the embedded length ratio increases. The effect of L/H is important in the case of thin piled walls. On the other hand, the wall thickness ratio, D/H , is more significant on maximum shear force ratios. The larger piled wall thickness is related to the smaller maximum shear force ratio. Inversely, the ratio of maximum shear force increases when the thickness of the piled wall increases.



(a)



(b)

Figure 8 Design charts for ratio of maximum shear force ratios, a) V_{max}/s_uD vs. L/H b) V_{max}/s_uD vs. D/H

Maximum bending moment ratios

In the design, practitioners require knowledge of the bending moment in order to design the pile wall size and required reinforcements besides information of maximum shear force. The results of the bending moment are presented in terms of dimensionless parameter as the maximum bending moment ratio (M_{max}/s_uD^2). **Figure 9** shows the relationship between the maximum bending moment ratio and embedded length ratio and wall thickness ratio. The pattern of maximum bending moment is similar to

those of maximum shear force. The term $M_{\max}/s_u D^2$ increases as the term L/H increases. The effects of embedded length ratio are significant in the case of thin piled walls. In contrast, ratios of maximum bending moment are inversely proportional to wall thickness ratios. The effect of D/H on $M_{\max}/s_u D^2$ is significant in the case of deep embedded length ratio.

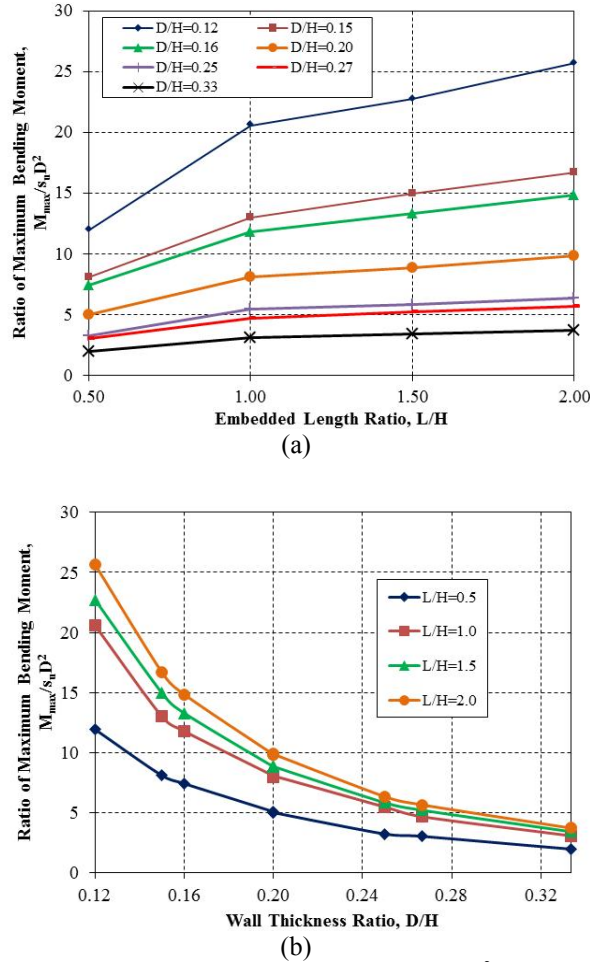


Figure 9 Design charts of maximum bending moment ratios, a) $M_{\max}/s_u D^2$ vs. L/H b) $M_{\max}/s_u D^2$ vs. D/H .

Figures 10 - 12 show examples of predicted failure mechanism, including results of deformed mesh and plastic points. Comparisons of failure mechanism are made for different ratios of D/H , but for same ratios of L/H . Generally, the failure mechanism looks similar to the classical circular-arc failure surface encountered in slope stability problems. The pile wall plunges and translates horizontally into the excavated side, while there is a rotational mechanism occurring about its top. The failure zone extends downward from the piled wall tip by the distance, L , and intersects the retained soil side about twice of the full wall length, $H+L$. This mode of failure corresponds to the deep-seated failure mechanism. The wall thickness effect also causes the failure zone to extend into the deeper zone of the lower soil and to extend laterally near the ground surface of the retained side. The failure zone extends to the excavated side about the embedment length, L .

Comparisons of predicted failure mechanisms between different ratios of L/H are shown in **Figures 13 and 14**. A similar failure mechanism can be observed in these 2 figures. Modes of failure consist of deep-seated circular failure zones, together with wall translation and rotation into the excavated side. The larger ratio of L/H is related to the larger failure zone in both horizontal and vertical directions. The failure mechanism of the smaller ratio of L/H is similar to that of the larger ratio. The former is just scaled up in terms of its failure size by a factor of 2.

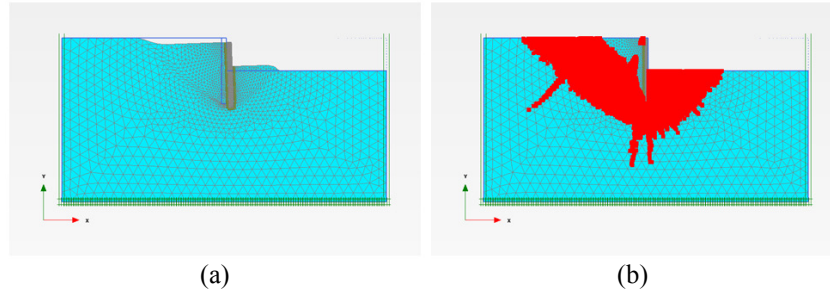


Figure 10 Failure mechanism where $D/H = 0.15$; $L/H = 1$, (a) deformed mesh, (b) plastic points.

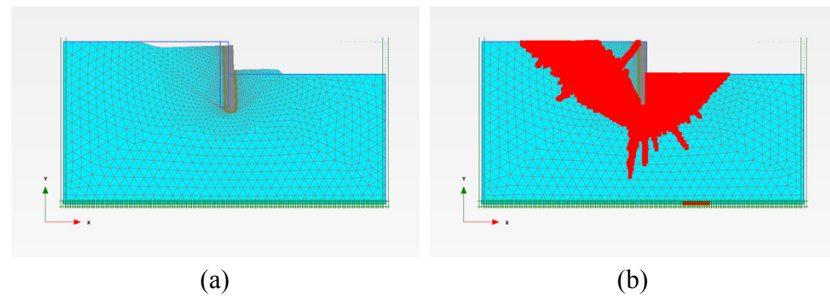


Figure 11 Failure mechanism where $D/H = 0.25$; $L/H = 1$, (a) deformed mesh, (b) plastic points.

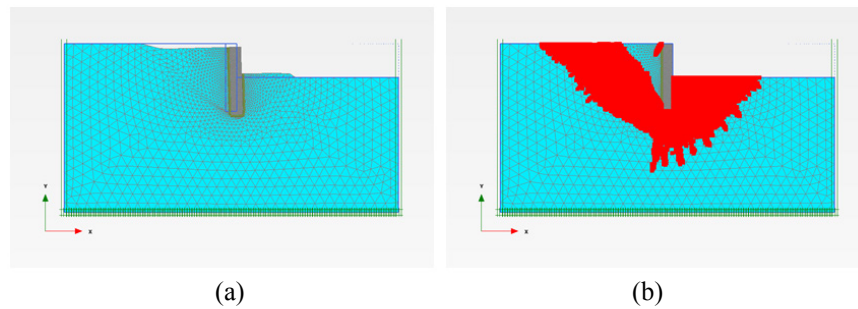


Figure 12 Failure mechanism where $D/H = 0.33$; $L/H = 1$, (a) deformed mesh, (b) plastic points.

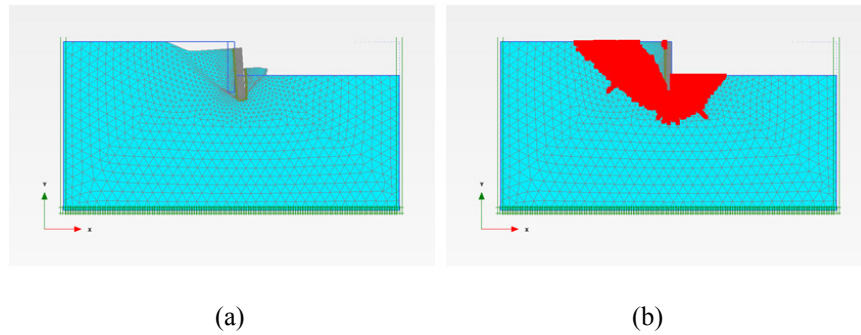


Figure 13 Failure mechanism where $D/H = 0.2$; $L/H = 0.5$, (a) deformed mesh, (b) plastic points.

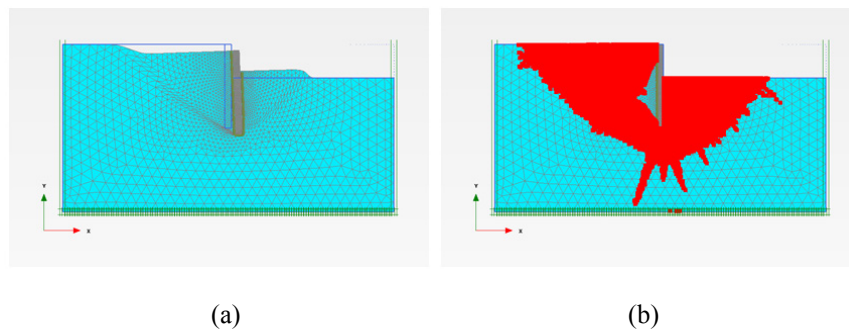


Figure 14 Failure mechanism where $D/H = 0.2$; $L/H = 1.5$, (a) deformed mesh, (b) plastic points.

Comparison between solid element and plate element modeling

Figure 15 shows comparisons of stability numbers of the piled wall between 2 cases with and without the effect of wall thickness. The former case corresponds to the volume element modeling of the piled wall, as described earlier. For the latter case, the piled wall is modeled by a plate element with an interface element around the wall. Therefore, the effect of wall thickness modeling can be distinguished by these 2 modeling approaches. It can be observed that the stability numbers of both cases are not the same. The differences in stability numbers are attributed to the wall thickness effect. Generally, stability numbers of the wall thickness cases are slightly higher than that of plate element case. Some significant difference in stability number can be observed when the ratio of D/H is high.

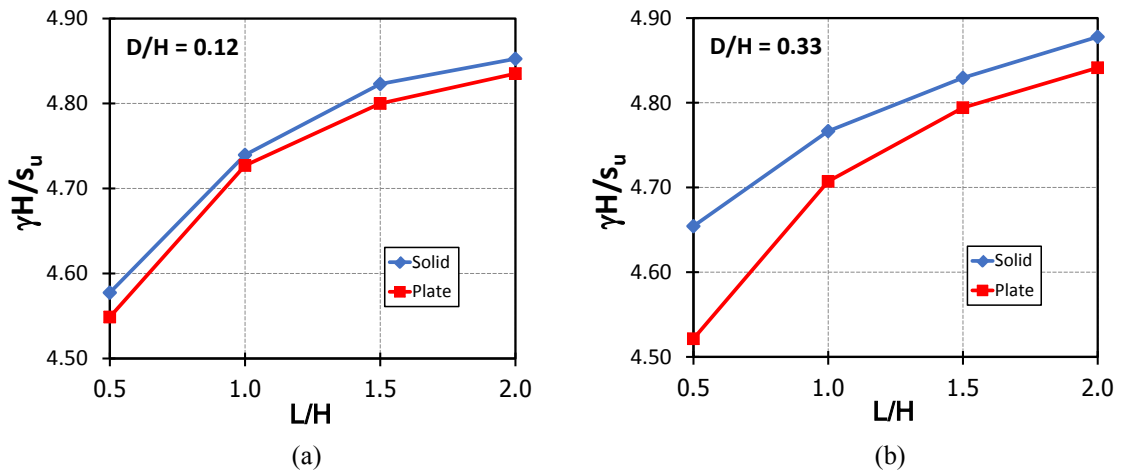


Figure 15 Comparison of stability numbers of the piled wall, (a) $D/H = 0.12$ (b) $D/H = 0.33$.

Comparison between the simulation results and the real field data

This section presents an application of the proposed design charts to analyze a case study of the piled retaining wall in practice. **Figure 16** shows the schematic geometry of the actual construction of the piled retaining wall in Bangkok (after Teparaksa *et al.* [13]). A piled wall with a diameter of 1.0 m, spacing of 1.1 m, and length of 18.0 m, was used as the retaining structure for the construction of the basement of a high-rise building in Bangkok. According to the soil data reported at this site, the average unit weight of clay, γ is 17.2 kN/m^3 and the average undrained shear strength, s_{ui} is 36.2 kN/m^2 . For the first excavation of 6m depth, there was no lateral bracing of the retaining piled wall. Hence, the piled wall behaved as the cantilever wall. Therefore, the proposed design charts can be used to analyze the stability of the first unsupported piled wall in this case.

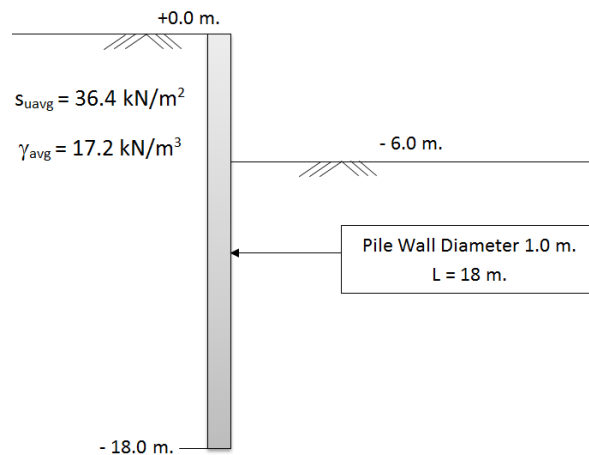


Figure 16 Schematic geometry of the actual construction of piled retaining wall in Bangkok

In order to apply the proposed design charts, the following input parameters must be determined: the excavated height, $H = 6$ m; the embedded length, $L = 12$ m; the wall thickness, $D = 1$ m; the pile spacing, $S = 1.1$ m. Thus, the dimensionless parameters of this problem can be calculated as: $L/H = 2$; $D/H = 0.17$. Using these dimensionless variables, the output dimensionless parameters, including the stability number, the ratio of maximum shear force, and the ratio of maximum bending moment, can be estimated from the proposed design charts in **Figures 7 - 9** as;

$$\gamma H/s_u = 4.86 \quad (5)$$

$$V_{\max}/s_u D = 3.20 \quad (6)$$

$$M_{\max}/s_u D^2 = 15 \quad (7)$$

It should be noted that the term of the undrained shear strength, s_u , in all proposed design charts is denoted as the mobilized undrained shear strength, which is required to maintain the stability of the problem. As a result, the FS can be calculated by the conventional definition used in slope stability analysis as the ratio of the full undrained shear strength (s_{ui}) to the mobilized undrained shear strength (s_u), as shown in Eq. (1).

Substituting $\gamma = 17.2$ kN/m³, $H = 6$ m, $s_{ui} = 36.4$ kN/m², into Eqs. (5) - (7), the mobilized undrained shear strength, the factor of safety, the maximum shear force (V_{\max}), and the maximum bending moment (M_{\max}) can be obtained as follows;

$$s_u = 21.23 \text{ kN/m}^2 \quad (8)$$

$$FS = 1.71 \quad (9)$$

$$V_{\max} = 3.2s_u D = 67.95 \text{ kN/m} \quad (10)$$

$$M_{\max} = 15s_u D^2 = 318.52 \text{ kNm/m} \quad (11)$$

Thus, the calculations evaluate that the first unsupported piled wall of this site is marginally stable, with a factor of safety of 1.71.

Assuming that the load factor of geotechnical problems is equal to 2, the applied ultimate maximum shear force (V_{umax}) and the applied ultimate maximum bending moment (M_{umax}) for one pile can be obtained as follows;

$$V_{\text{umax}} = 2V_{\max}S = 149.49 \text{ kN} \quad (12)$$

$$M_{\text{umax}} = 2M_{\max}S = 700.70 \text{ kNm} \quad (13)$$

Based on the data of the piled wall reported in Teparaksa *et al.* [13], the piled wall was reinforced with steel reinforcements and stirrups, so that the shear capacity (V_n) and the moment capacity (M_n) of the section are given as;

$$V_n = 251.50 \text{ kN} \quad (14)$$

$$M_n = 820.00 \text{ kNm} \quad (15)$$

Thus, it can be verified that the section of the piled wall has enough capacities of the shear force and the bending moment to resist the applied ultimate maximum shear force and moment by applying the strength reduction factors (ϕ) for shear force ($\phi = 0.85$) and moment ($\phi = 0.9$) for V_n and M_n as follows;

$$\phi V_n = 0.85(251.50) = 213.78 \text{ kN} > V_{\text{umax}}, \text{ Design Safe} \quad (16)$$

$$\phi M_n = 0.9(820.00) = 738.00 \text{ kNm} > M_{\text{umax}}, \text{ Design Safe} \quad (17)$$

Based on the above demonstration, it can be seen that the proposed design charts can be conveniently and efficiently employed to evaluate the stability of unsupported piled retaining walls and to check the section capacity of piled walls without the need for finite element analysis.

Conclusions

This paper presents numerical solutions of the undrained stability of a cantilever piled wall in cohesive soil. A literature review shows that there are few studies of this topic, but there is increased use of this type of retaining wall in practice nowadays. Parametric studies of the retaining piled wall are performed by 2 dimensional plane strain finite element analysis. The limit state calculations by the finite element analyses are simulated by the strength reduction method. In this paper, the piled wall is modeled with volume element in contrast to conventional modeling by plate element. Therefore, the effect of wall thickness can be studied by this realistic modeling. Results are summarized in the form of input dimensionless parameters as: embedded length ratio (L/H) and wall thickness ratio (D/H). The design charts are developed for 3 output dimensionless parameters as: stability number ($\gamma H/s_u$), ratio of maximum shear force ($V_{\text{max}}/s_u D$), and ratio of maximum bending moment ($M_{\text{max}}/s_u D^2$). The effects of dimensionless parameters, L/H and D/H , on $\gamma H/s_u$, $V_{\text{max}}/s_u D$, $M_{\text{max}}/s_u D^2$ depend on their ratios; whether both of them are small or large in the same direction or in the opposite direction. Predicted failure mechanisms indicate that the failure of the system is caused by the translation and rotation of the piled wall into the excavated side. The failure shape and zone look like the circular-arc failure mechanism or deep-seated failure mechanism usually assumed in slope stability analyses. In practice, proposed design charts make it possible to analyze and design cantilever piled walls with one row or several consecutive piled rows. Classical approximation of piled walls as plate element may not correspond to the actual problem. In particular, this approximation may be serious in some cases, such as cases where there is a larger size of piled wall and several pile rows are used to construct retaining structures. As a result, a more realistic analysis and design can be performed easily and efficiently with proposed design charts, as demonstrated in the back analysis of a selected case study.

References

- [1] N Thasnanipan, MA Win and T Boonyarak. Minimizing ground movement by using deep soil mixing technique. *In: Proceeding of the 12th National Convention on Civil Engineering*. Phitsanulok, Thailand, 2007. p. 240-6.
- [2] K Terzaghi. *Theoretical Soil Mechanics*. Wiley, New York, USA, 1943.
- [3] L Bjerrum and O Eide. Stability of strutted excavations in clay. *Geotechnique* 1956; **6**, 115-28.
- [4] O Eide, G Aas and T Josang. Special application of cast-in-place walls for tunnels in soft clay. *In: Proceeding of the 5th European Conference on Soil Mechanics and Foundation Engineering*. Madrid, Spain, 1972, p. 485-98.
- [5] TD O'Rourke. *Base Stability and Ground Movement Prediction for Excavations in Soft Clay*. Retaining Structures 1993, Thomas Telford, London, p. 131-9.
- [6] B Ukritchon, AJ Whittle and SW Sloan. Undrained stability of braced excavation in clay. *J. Geotech. Geoenviron. Eng.* 2003; **129**, 738-55.
- [7] VN Khatri and J Kumar. Stability of an unsupported vertical circular excavation in clays under undrained condition. *Comput. Geotech.* 2010; **37**, 419-24.
- [8] CM Martin. The use of adaptive finite-element limit analysis to reveal slip-line fields. *Geotechnique Lett.* 2011; **1**, 23-9.
- [9] RBJ Brinkgreve. *Plaxis 2D 2012*. PLAXIS company, The Netherlands.

- [10] GM Filz and MP Navin. *Stability of Column-Supported Embankments*. Report of the Virginia Department of Transportation, 2006.
- [11] H Yang. Experimental study on mechanical property of soil-cement. *In: Proceeding of the 2nd International Conference on Electronic & Mechanical Engineering and Information Technology*. Liaoning, China, 2012, p. 790-3.
- [12] R Butterfield. Dimensional analysis for geotechnical engineering. *Géotechnique* 1999; **49**, 357-66.
- [13] W Teeparaksa, P Sontiprasart, N Prachayaset and S Keawsawasvong. Performance of contiguous pile wall with raking strut for basement construction of BITEC Phase 2 project. *In: Proceeding of the 28th KKHTCNN Symposium on Civil Engineering*, Bangkok, Thailand, 2015.